Understanding JET-C quiescent phases with edge harmonic magnetohydrodynamic activity and comparison with behaviour under ITER-like wall conditioning

To cite this article: D Brunetti *et al* 2022 *Plasma Phys. Control. Fusion* **64** 044005

OPEN ACCESS
IOP Publishing
Plasma Physics and Controlled Fusion
Plasma Phys. Control. Fusion **64** (2022) 044005 (12pp)
https://doi.org/10.1088/1361-6587/ac4d3a

Understanding JET-C quiescent phases with edge harmonic magnetohydrodynamic activity and comparison with behaviour under ITER-like wall conditioning

D Brunetti[1,*], C J Ham[1], J P Graves[2], E Lazzaro[3], S Nowak[3], A Mariani[4], C Wahlberg[5], W A Cooper[6], E R Solano[7], S Saarelma[1], L Frassinetti[8], M Fontana[2,11], A Kleiner[9], G Bustos Ramirez[2], E Viezzer[10] and JET Contributors[12]

[1] UKAEA-CCFE, Culham Science Centre, Abingdon, Oxon OX14 3DB, United Kingdom
[2] École Polytechnique Fédérale de Lausanne (EPFL), Swiss Plasma Center (SPC), CH-1015 Lausanne, Switzerland
[3] Istituto per la Scienza e Tecnologia dei Plasmi CNR, Via R. Cozzi 53, 20125 Milan, Italy
[4] Dipartimento di Fisica 'G. Occhialini', Università di Milano-Bicocca, Milan, Italy
[5] Department of Physics and Astronomy, Uppsala University, PO Box 516, SE-751 20 Uppsala, Sweden
[6] Swiss Alps Fusion Energy (SAFE), CH-1864 Vers l'Eglise, Switzerland
[7] Laboratorio Nacional de Fusión, CIEMAT, Madrid, Spain
[8] Division of Fusion Plasma Physics, KTH Royal Institute of Technology, Stockholm, SE, Sweden
[9] Princeton Plasma Physics Laboratory, Princeton University, Princeton, NJ 08543, United States of America
[10] Department of Atomic, Molecular and Nuclear Physics, University of Seville, Avda. Reina Mercedes, 41012 Seville, Spain

E-mail: daniele.brunetti@ukaea.com

Received 6 October 2021, revised 17 December 2021
Accepted for publication 20 January 2022
Published 18 February 2022

Abstract

An analysis of edge localised mode-free (quiescent) H-mode discharges exhibiting edge harmonic magnetoydrodynamic activity in the JET-carbon wall machine is presented. It is observed that the otherwise quiescent pulses with multiple-*n* harmonic oscillations are sustained until a threshold in pedestal electron density and collisionality is crossed. The macroscopic pedestal parameters associated with the quiescent phase are compared with those of a database of JET-ELMy discharges with both carbon and ITER-like wall (ILW). This comparison provides the identification of the existence regions in the relevant pedestal and global plasma parameters for edge harmonic oscillations (EHOs) in JET plasmas. Although the ELMy

[11] Present address: UKAEA-CCFE Culham Science Centre, Abingdon, Oxon OX14 3DB, United Kingdom.
[12] See the author list of 'Overview of JET results for optimising ITER operation' by Mailloux *et al* to be published in Nuclear Fusion Special Issue: Overview Summary Papers from the 28th Fusion Energy Conference (Nice, France 10–15 May 2021).
[*] Author to whom any correspondence should be addressed.

database scans pedestal collisionality and β values typical of ET-carbon quiescent operation, shaping and current are not simultaneously compatible with EHO existence. Nevertheless, ILW operation with JET-carbon quiescent-like parameters could in principle be achieved, and improved pedestal performance could be observed in more recent JET-ILW pulses.

Keywords: tokamak, JET, QH-mode, EHO, ELMs

(Some figures may appear in colour only in the online journal)

1. Introduction

The most promising scenarios for achieving efficient controlled thermonuclear fusion in tokamak machines are the so called high-confinement (H-mode) regimes. Such scenarios show long energy confinement times and are typically characterised by the presence of sharp and narrow plasma edge pedestals, both in mass density and temperature. Unfortunately, the associated strong radial gradients favour the appearance of short wavelength magnetohydrodynamic (MHD) perturbations called edge localised modes (ELMs) [1]. These sudden and violent events are associated with rapid energy and particle expulsions which deposit intolerable heat loads on plasma facing components. In addition to severe plasma contamination, ELMs can significantly reduce machine lifetime. Therefore, it is of crucial interest to attain high-performance scenarios without the deleterious presence of ELMs [1].

One of the most promising intrinsically ELM-free regimes is the so called quiescent H-mode. In this regime, which shares with the standard H-mode large edge pressure gradients and long energy confinement times, ELMs are avoided and replaced by continuous low-n mild MHD perturbations, and the associated peak energy and heat loads on the plasma facing materials are significantly lower compared to ELMy regimes. These edge harmonic oscillations (EHOs) are well localised within the edge region of large gradients (pedestal) and feature multiple n toroidal harmonics with a rather long lifetime, of the order of 1 s [2]. EHOs have been observed in DIII-D, ASDEX-U, JT60 [3–6], and JET [7]. In [7] such oscillations are called Outer Modes. Since the MHD dynamics described in [3, 4, 7]. have the same characteristics, for the sake of clarity, hereafter we will refer to such oscillations as EHOs[13]. As observed in [7], EHOs have several common features with the low-n type-I ELM precursors studied in [10].

It is observed that EHOs in JET are prone to develop in the early phase of the discharge, during the density ramp when ion and electron temperatures reach their highest values at the pedestal top. It is also observed that above a critical value of the pedestal density ($\sim 5 \times 10^{19}$ m^{-3}) the quiescent phase with EHOs abruptly ends and ELMs appear. We point out that quiescent regimes in DIII-D, ASDEX-U and JT60-U experiments [3–6] usually operate with lower values of the pedestal top density compared with JET, typically three or four times smaller. Although for some discharges EHOs can re-emerge after an ELM crash, the quiescent phase is not usually recovered after the first ELM is triggered.

Thus, the aim of this paper is to detail and characterise the existence conditions for EHOs in JET, in order to determine the pedestal features required to guarantee the accessibility to quiescent regimes with EHOs, and potentially in machines with a metallic wall. These existence conditions are assessed by comparing global and pedestal parameters, namely electron β, collisionality, q_{95} and triangularity, of quiescent with EHOs (Q-EHO) shots with the ones extracted from a carbon (C) and ITER-like wall (ILW) EUROfusion pedestal database of ELMy discharges [11, 12]. It is found that the operational regime of Q-EHO plasmas identified by the parameters given above does not overlap the one explored by the ELMy database. This holds in particular for ILW plasmas where the electron temperature, which plays a crucial role, is significantly smaller compared to carbon wall discharges. We finally point out that some indications of brief edge coherent activity have been observed in recent hybrid JET-ILW shots with high pedestal performance. Although these oscillations have been observed transiently, efforts are now focussed on steadily sustaining this behaviour in metal machines [13].

Thus, the paper is organised as follows: In section 2 we describe the JET-C experimental set-up and the typical features of the EHOs which are observed during the quiescent phase. In section 3 we analyse a database of JET discharges with a carbon and ILW, which although exhibiting quiescent compatible pedestal parameters are in ELMy regime. This is done by inspecting the associated physical global and pedestal parameters (e.g. collisionality, temperature, etc). These parameters are then compared with the ones observed in the Q-EHO JET-C pulses analysed in section 2. By assessing the differences between JET-C plasmas with EHOs and the ELMy database, we infer the conditions that have to be met to achieve quiescent operation, and in particular whether such conditions are compatible with a metallic wall. Finally, a discussion of the results and concluding remarks are given in section 4.

2. JET-C quiescent discharges with EHO activity

2.1. Experiment and analysis setup

We analyse a set of four JET-C discharges showing a quiescent ELM-free phase in which coherent edge EHOs are observed. These pulses feature a hot-ion H-mode phase [7, 14], obtained by reducing particle fuelling from external sources and wall with an initial operation at low plasma density and fairly high

[13] Historically, Outer Modes refer to low-n (mainly $n = 1$) MHD oscillations with frequencies $\sim$10 kHz observed typically within the outer 20% of the plasma [8, 9] (broader compared to EHOs). In [9], Outer Modes refer to current driven external kinks.

Table 1. Macroscopic global plasma parameters for four JET-C discharges with EHO activity. Triangularity is computed by averaging between its upper and lower values. For each pulse, β_N, q_{95}, κ, and δ are averaged over time window $t_1 - t_2$. Note the ≈30% reduction in the injected NBI power in #79455. Shaping, i.e. κ, and δ, and q_{95} take similar values across the four pulses.

Shot #	B_t (T)	I_p (MA)	NBI (MW)	β_N	t_1 (s)	t_2 (s)	t_{ELM} (s)	q_{95}	κ	δ
75411	2.7	2.5	15.3	1.94	14	16	15.4	3.37	1.72	0.41
78012	2.7	2.5	16.8	1.87	13.6	16	14.65	3.36	1.73	0.39
78014	2.7	2.5	16.7	1.98	13.8	16	14.23	3.38	1.73	0.41
79455	2.7	2.5	11	1.67	14	16	14.85	3.3	1.71	0.40

co-current NBI power yielding very high ion temperatures. This was specifically designed for achieving high pedestal temperatures. Bolometry and D_α emission confirm the ELM-free phase, and the EHO identification is achieved by matching the mode rotation frequency inferred from magnetic signals with the one obtained by edge electron temperature fluctuation measurements [15] (see the next subsection for further details). This provides a unique mode identification for toroidal spectral structure and spatial localisation.

The requirements for the pulse selection are (i) a relatively long quiescent phase duration, and (ii) diagnostic signal clarity, i.e. all of the EHO footprints must be clearly visible on all the relevant diagnostics. The pulse numbers of the four discharge analysed in this work are listed in table 1, which also reports the vacuum toroidal field B_t at the plasma geometric centre, the plasma current I_p, β_N (see [3] for the definition), q_{95}, elongation κ and triangularity δ. The NBI input power is also given, as well as the time window $t_1 - t_2$ within which the analysis is performed. The EHO appears approximately at t_1, whereas t_{ELM} indicates the time when the quiescent phase with EHOs is lost and the plasma enters the ELMy regime. At time t_2 the plasma is deep into the ELMy phase. Other quiescent discharges sharing very similar features with the ones reported in table 1 with a likely EHO activity, have not been analysed because of the lack of clarity on some of the diagnostics signals.

Error field correction coils (EFCCs) for ELM control were employed in discharges #78012 and #78014. In both pulses the coil current was ramped up and down in 100 ms, with the current flat-top of ±0.5 and ±1 kA for shots #78012 and #78014 respectively lasting from $t = 14.1$ s to $t = 15.9$ s (the plus/minus sign refers to 1–5/3–7 octants). No EFCCs were employed in pulses #75411 and #79455. The ICRH heating is switched on only at the very end of each pulse, so that we regard these shots as Ohmically and NBI heated.

All pulses in table 1 exhibit similar behaviour, in which the electron temperature increases all across the plasma core region during the early phase when the NBI is switched on, and whose power is steadily maintained for the whole discharge (cf figure 8 in section 2.3). At the same time, the plasma density n_e is ramped up, reaching the stationary core value $>7-8\times10^{19}$ m^{-3}. The value of the pedestal density rises accordingly, as shown in figure 1 from high resolution Thomson scattering (HRTS) measurements. The corresponding values of ion (charge exchange) and electron (HRTS) pedestal temperatures, T_i and T_e respectively, are shown in figure 2. Details on the definition of pedestal quantities, e.g. height and

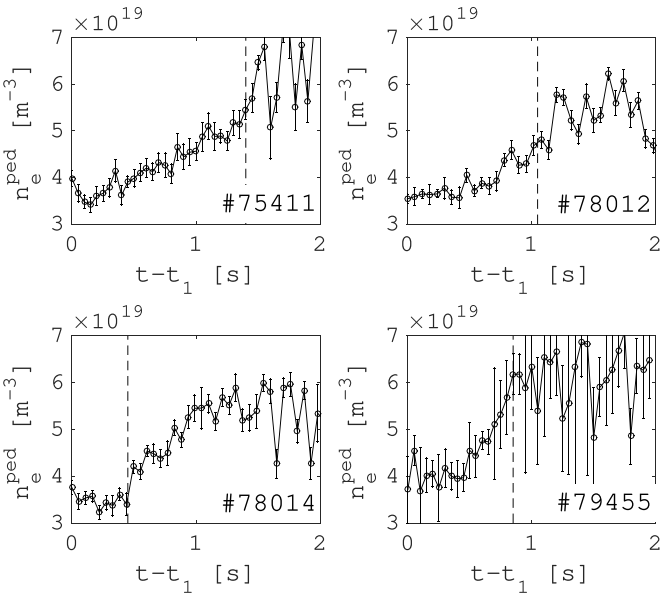

Figure 1. Evolution of the pedestal density for the discharges of table 1. A steady increase in n_e^{ped} is observed. The dashed vertical lines in each plot indicate the appearance of the ELM after which the Q-EHO phase is lost. Note the large errorbars in the pedestal density value after the first ELM in shot #79455 (errorbars are obtained by a weighted fit of HRTS data).

width, are detailed in [16]. The density rise is accompanied by an increase of the effective charge Z_{eff} which ranges approximately from 1.8 to 2 during the quiescent phase, whereas during the ELMing stage reaches values up to 2.5. We observe that in pulse #78014, the EHO disappears at $t = 14.23$ s despite the low pedestal density, and a sudden increase of n_e^{ped} occurs after the appearance of the first ELM. The EHO loss may be caused by variations in the global temperature profile which are not captured by the local pedestal analysis (see section 2.5).

As the mass density is ramped up, the toroidal rotation v_{tor} (obtained from charge exchange measurements, cf figure 3) is observed to reduce whereas β_N remains approximately constant. Note that in JET the NBI is co-current [17]. In the time window indicated in table 1, ion and electron temperatures tend to decrease, with T_i exhibiting smaller gradients in the pedestal compared with T_e. T_i and v_{tor} are found to have similar radial dependencies. We point out that during the quiescent phase the ion temperature at the pedestal top is slightly larger on average compared with T_e, the former taking values

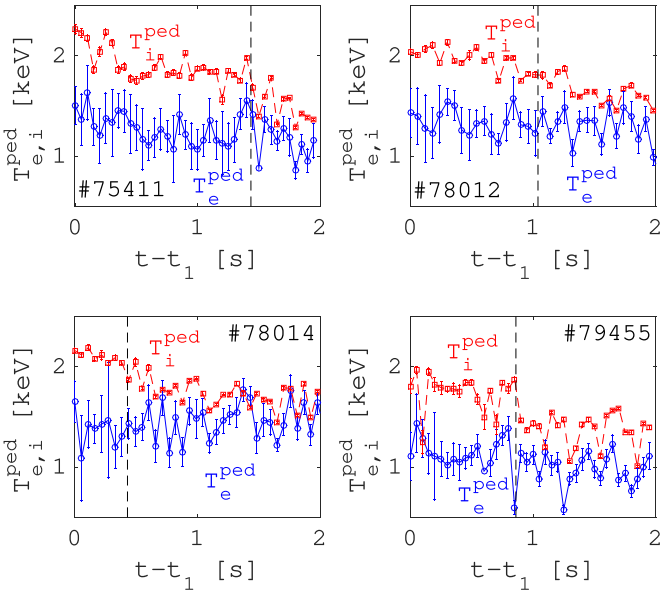

Figure 2. Evolution of the pedestal ion (red) and electron (blue) temperatures for the discharges of table 1. T_i is obtained from charge exchange measurements, whereas T_e from HRTS. Note that the ion temperature has a more pronounced decrease during the pulse evolution compared to T_e.

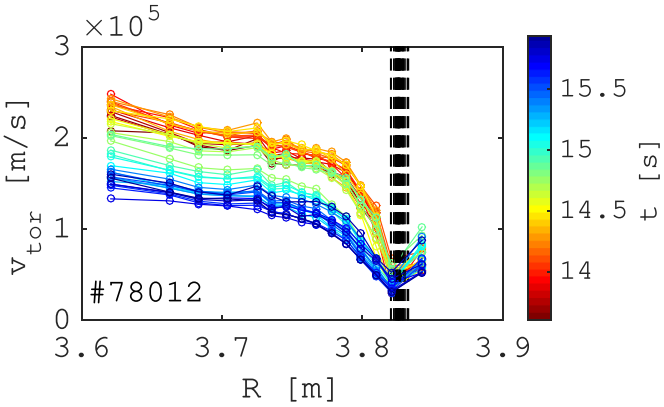

Figure 3. Time evolution of the toroidal (C) rotation profile for discharge #78012 from charge exchange measurements in the time window indicated in table 1 (early times in red, later ones in dark blue). Error bars are not shown for the sake of visual clarity. A steady decrease of the core rotation frequency is observed. Note that the separatrix position is allowed to vary within the region delimited by the dashed vertical line.

of about 2 keV whereas the latter is ∼1.4–1.5 keV at the EHO onset. The two temperatures get closer after the appearance of the first ELM.

2.2. Characterisation of MHD dynamics

Very rich MHD dynamical behaviour is observed during the early NBI heating phase as clearly shown in figure 4. EHOs however behave similarly in all four shots of table 1 with a lifetime of ∼0.5–1 s. In pulse #78014, after an internal (core) temperature crash at $t = 13.68$ s, a steady EHO is sustained

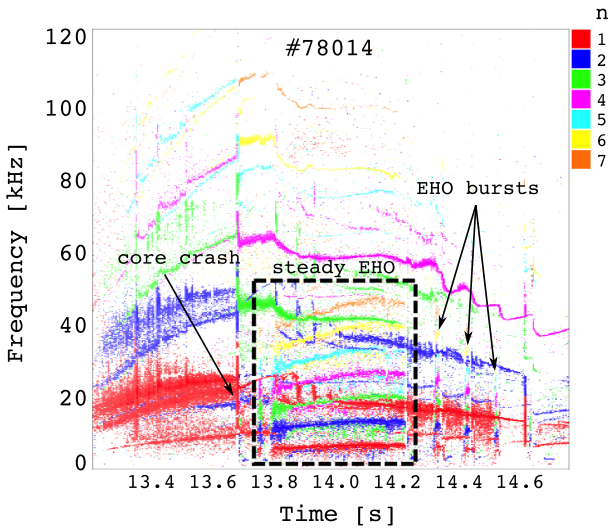

Figure 4. MHD mode analysis inferred from high bandwidth pick-up coils signals of the early phase of discharge #78014. After an internal temperature crash at $t = 13.68$ s, a MHD activity with multiple harmonics up to $n = 7$ is observed from $t = 13.8$ s to $t = 14.2$ s (highlighted in the dashed box). Brief coherent MHD bursts localised in the pedestal region appear before ELM crashes at 14.35, 14.45 and 14.53 s, resembling the type-I ELM precursor activity discussed in [10].

for ∼400 ms starting at $t = 13.8$ s (cf table 1). Each toroidal harmonic with mode number n of the EHO rotates with frequency $n\Omega^{ped}$ where Ω^{ped} is the rotation frequency at the pedestal top [7]. After the steady EHO phase is lost, short lived pre-ELM EHO bursts with multiple low-n harmonics appear from 14.3 to 14.5 s. We point out that similarities between EHOs (or Outer Modes) and the low-n ELM precursors studied in [10] have been pointed out in [7]. The latter appear as multiple n coherent oscillations localised at the plasma boundary, and were observed frequently in hot-ion H-mode regimes [10]. The poloidal spectral structure of these low-n ELM precursors features poloidal mode numbers comparable or slightly larger than q_{95}, and we expect EHOs to have similar characteristics. Indeed, as described in [7], the magnetic signal was found to have a strong $m = 4$ component. Note that this is also consistent with recent findings in [18], where a thorough description of the magnetic spectrum is given.

During the density ramp-up, when the electron temperature is the highest, a clear signature of multiple n harmonics all equally spaced in the frequency domain appear on the magnetic diagnostics. In order to assess the radial location of these MHD modes, and therefore identify their EHO-like nature, in analogy with [5, 15] the magnetic measurements are compared with the electron cyclotron emission (ECE) signals. The EHO is uniquely identified by matching the rotation frequencies of the various harmonics measured by the two diagnostics. The ECE channel distribution and location in the major radius of the outer midplane is given in figure 5. Note that for all the shots listed above, channels 54 and 66 are usually associated with pedestal measurements (odd number channels were not available).

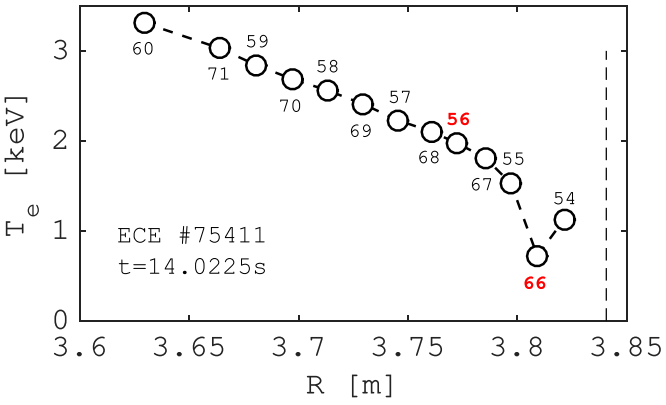

Figure 5. Temperature profile of shot #75411 showing the major radius location of the ECE lines of sight. Note that in all discharges listed in table 1, the pedestal ECE emission is, with a good approximation, associated with channel 66 (highlighted in red). Channel 56 is the nearest-non pedestal channel, so that it is always inspected to check the edge mode localisation. It is important to point out that even channels only are associated with the fast ECE data acquisition. The separatrix position is denoted by the dashed vertical line.

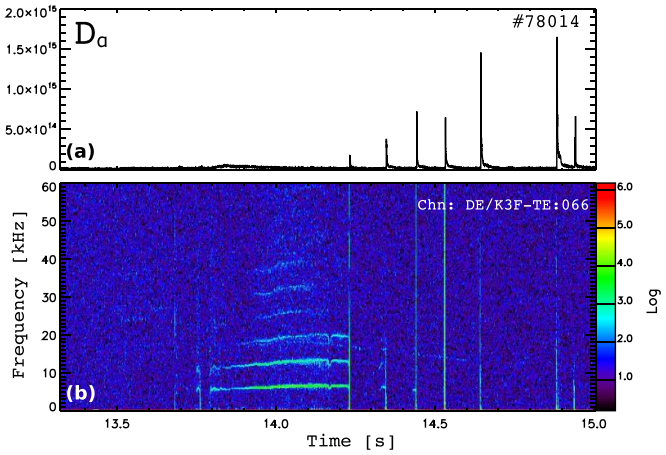

Figure 6. Time trace of the D_α outer divertor signal (a) and the ECE emission channel 66 (b) for JET discharge number #78014. The EHO lasts for approximately 400 ms from $t = 13.8$ s to $t = 14.2$ s. The ECE signals (colourbar in log scale) have to be compared with the magnetics shown in figure 4.

A typical spectrogram of ECE near-pedestal signals (channel 66 of figure 5) is shown in figure 6. The electron temperature fluctuation with the many-n harmonic structure displayed in figure 4 is clearly recognisable. It is found that the ECE signal does not propagate further beyond the pedestal shoulder. Indeed, as clearly shown in figure 7, the ECE trace of the EHO is not visible inside channel 56 which is the first available channel in the core region outside the pedestal. DIII-D and JT60-U experiments [6, 19] also reported similar behaviour, which resembles the dynamics of low-n ELM precursors studied in [10]. These fluctuations have been shown to be localised within the pedestal radii and not to extend radially beyond the pedestal shoulder, giving us confidence on the pedestal

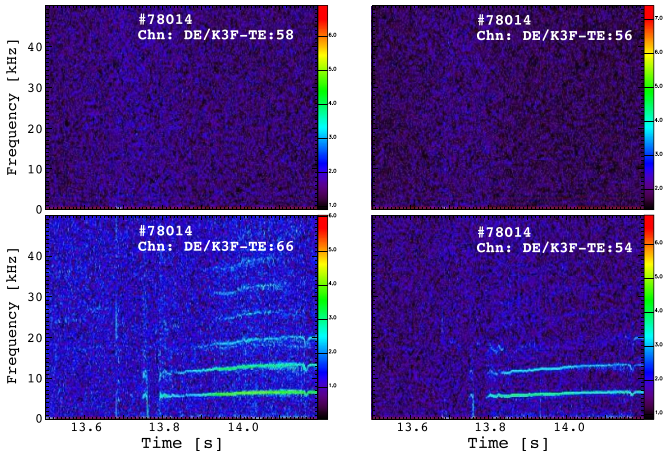

Figure 7. Spectrogram of the ECE emission (colourbar in log scale) for channels 54, 56, 58 and 66 (cf figure 5) for shot #78014.

radial localisation of the EHO in JET, which must indeed be extremely narrow.

It is worth noting that EHOs in DIII-D, ASDEX-U and JT60 have been observed in low pedestal density plasmas of the order of 1×10^{19} m^{-3} and currents of 1 MA [3–6], whereas JET quiescent plasmas can be sustained up to fairly large values of the pedestal density ($n_{e,crit}^{ped} \sim 5 \times 10^{19}$ m^{-3}, cf figure 1). Although JET operates at higher plasma current, this behaviour is not fully explained as local quantities such as collisionality, the electron β_e, Z_{eff} seem to be comparable across these machines [4, 20].

Furthermore, we notice that EHOs are not affected by external magnetic perturbations, at least up to 1 kA of EFCC current. Indeed, the EHO dynamics observed in discharges #75411 and #79455 with no active EFCCs, is essentially equivalent to the one of pulses #78012 and #78014 in which EFCCs were applied. Also, in shots #78012 and #78014, EHOs occur well before EFCCs are applied at ∼14 s, and disappear well before the EFCC current is switched off at $\sim t_2$. This suggests that the EHO must be driven primarily by internal, i.e. within the last closed flux surface, mechanisms.

It is worth pointing out that the ELM appearance does not necessarily imply that the quiescent regime cannot be recovered. Indeed, in discharge #78012 a first quiescent phase lasts until $t \approx 14.3$ s when an ELM occurs and the EHO is lost; after this ELM event, the EHO appears again at $t \approx 14.45$ s and lasts until t_{ELM}. In pulse #79455 instead, the EHO disappears spontaneously at $t \approx 14.64$ s, whereas the quiescent state persists until $t = t_{ELM}$.

2.3. *The role of plasma rotation*

We now argue that the toroidal rotation affects weakly the appearance of EHOs. This is because we observe that the toroidal rotation frequency at the pedestal top drops *after* the appearance of the first ELM as shown in figure 8, which also indicates that EHOs exist within a wide range of pedestal rotation frequencies. Moreover, although a connection between

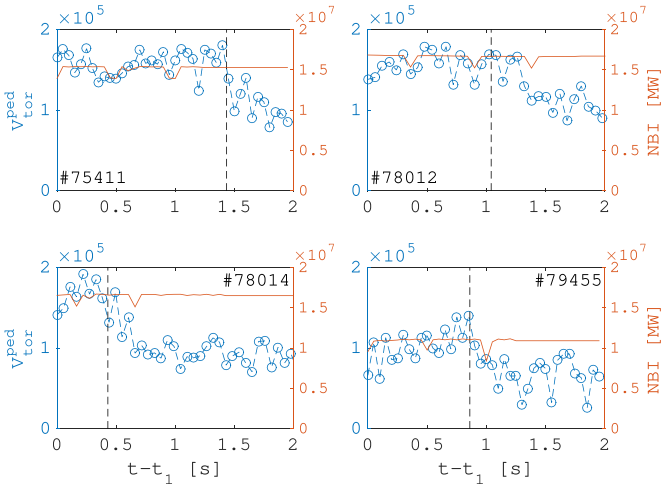

Figure 8. Toroidal rotation at the pedestal top (computed by averaging density and electron temperature pedestal positions) and NBI power for the four shots of table 1. Note that, despite the steady NBI power, a drop in the rotation pedestal value occurs at the appearance of first ELM, indicated by the dashed vertical line, after which the EHO phase is lost.

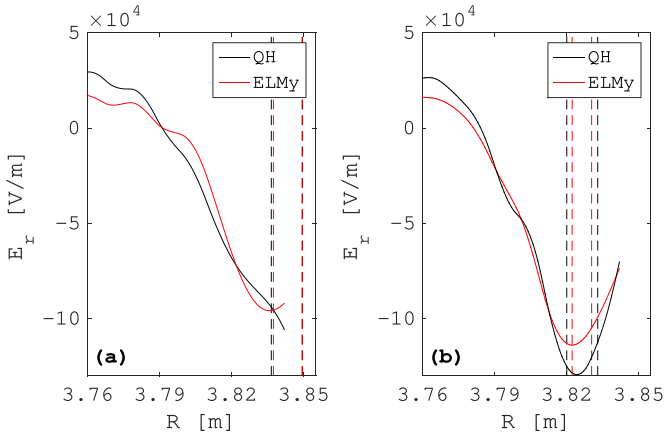

Figure 9. Radial electric field for pulses #75411 (a) and #78012 (b) during the quiescent (black, averaged over $t_1 - t_{ELM}$) and ELMy (red, averaged over $t_{ELM} - t_2$) phases. The separatrix position varies within the region indicated by the two vertical dashed lines (same colour meaning as for E_r). E_r has been calculated up to $R = 3.8425$ m for which averaged T_i data are available.

toroidal (carbon) rotation shear and Q-EHO phase was established in [7], DIII-D results of [21] show that the accessibility of the quiescent phase is almost independent of the toroidal (carbon) rotation shear. It is also worth stressing that there could be a consistent difference between carbon and main-ion species rotation profiles in the pedestal region, the latter exhibiting significantly weaker gradients [22–24]. As such, the rotation of the carbon impurity may not be a good proxy for inferring the main ion rotation properties. Furthermore, non-linear MHD simulations with the JOREK code [25] found that toroidal flows have a weak effect on the destabilisation and saturation of modes which might be related to a Q-EHO phase. Interestingly, we notice that similar edge localised oscillations with a dominant $n = 1$ component have been recently reported in Alcator C-Mod in low-collisionality and high pressure pedestal regimes [26]. No NBI was employed in the C-Mod experiments [26], supporting our claim that these edge fluctuations do not depend explicitly on plasma toroidal rotation. In conclusion, the experimental evidence in JET, also supported by the results presented in [6, 21] and numerical modelling, gives us confidence that other physical effects might be more relevant for the EHO appearance.

2.4. Radial electric field during the quiescent and ELMy phases

As pointed out in [21], one of the key parameters which determine the accessibility to the quiescent phase is the edge $E \times B$ flow shear. This flow manifests itself as a plasma rotation mainly in the poloidal direction, and its strength is proportional to the radial electric field. From the radial ion force balance equation [27], allowing for plasma shaping through elongation, we have near the edge

$$E_r \approx \sqrt{\frac{2}{1+\kappa^2}}\left(\frac{dp_i/dr}{en_i} + \frac{a\kappa B_t}{q}\Omega_{tor}\right) - v_{pol}B_t,$$

where $p_i = n_i T_i$ with n_i the ion density, e the ion electric charge, κ the plasma elongation, a and R_0 the minor and major radii respectively, $\Omega_{tor} = v_{tor}/R$ the toroidal angular frequency, v_{pol} the poloidal velocity and r a flux label (for the geometry of the beam injection and sign conventions we refer to [17, 28]). Writing $R = R_0 + r\cos\theta$, we have $d/dr = d/R$ at $\theta = 0$. This allows to simplify the analysis by taking all the relevant quantities as a function of R on the equatorial outer mid-plane. Figure 9 shows E_r averaged over the quiescent and ELMy time windows as a function of the major radius. The E_r well takes values comparable to those observed in DIII-D [19, 29] of the order of $\sim$100 kV m^{-1}, although no strong variations of E_r are observed when transitioning to the ELMy phase [30].

This finding suggests that in the four discharges of table 1, the pedestal density evolution should be the main actor responsible for transition from quiescent to ELMy regime. This, indeed, is discussed in the next subsection.

2.5. Pedestal density and temperature conditions for the Q-EHO phase accessibility

Thus, to further investigate what conditions favour the EHOs existence, we study the localisation of the discharges of table 1 in $n_e^{ped} - T_e^{ped}$ space. Figure 10 shows the instantaneous pedestal values of density and electron temperature during the time window $t_1 - t_2$ for the four shots considered. We observe that the Q-EHO phase exists in the region of low-density with temperatures $\gtrsim$1 keV. Note that most of the high pressure values associated with an ELMy pedestal belong to pulse #78014, and these may be connected with the EHO-like bursts prior to ELMs shown in figure 4. During the discharge, the plasma evolves towards an ELMy regime which loses the EHOs.

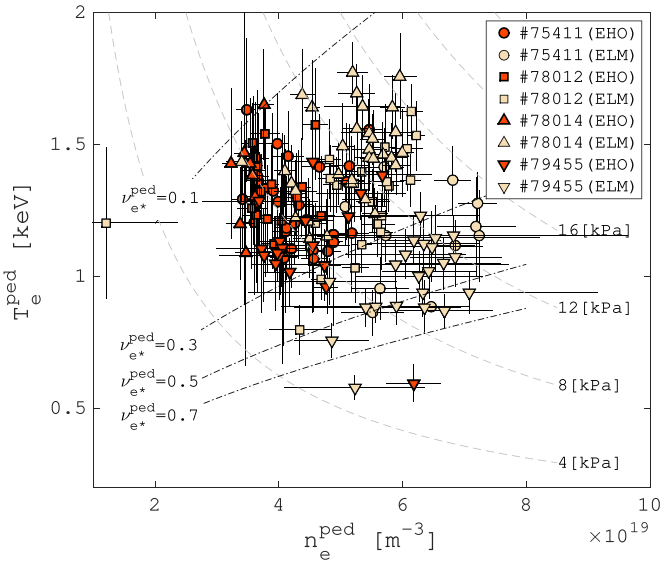

Figure 10. Scatter plot of the instantaneous pedestal values for density and electron temperature at the pedestal top for the discharges in table 1 during the selected time window (we point out that the pedestal position of n_e is approximately the same of the one of T_e). The red points refer to ELM-free phases with EHO activity. The constant electron pressure and collisionality level curves are also indicated, ν^{ped}_{e*} is computed by averaging $q_{95}, R_0, \kappa, Z_{eff}$ over the time window $t_1 - t_2$. EHOs tend to cluster in high temperature-low density regions.

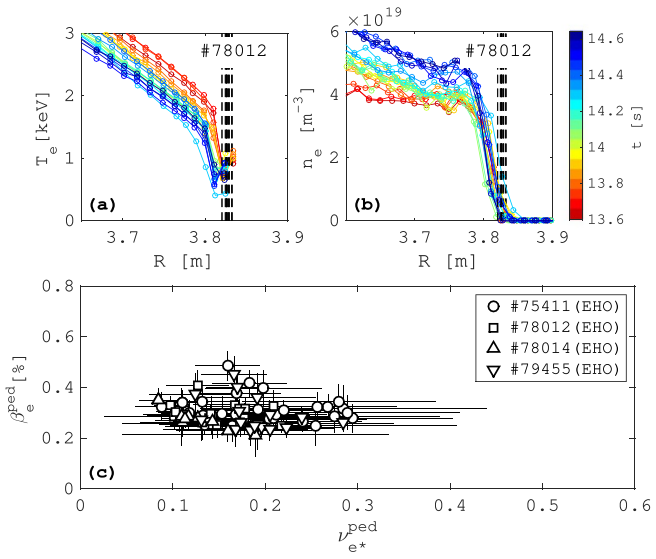

Figure 11. Electron temperature (panel (a), data from ECE) and density (panel (b), from HRTS) profiles of discharge #78012 for the time window $t_1 - t_{ELM}$ of table 1 (early times in red, later ones in dark blue). The separatrix position varies within the region identified by the vertical dashed lines. Note that for this discharge, T_e values from ECE are higher than the ones recorded by the HRTS diagnostic, although the radial profile remains the same. In (c), the instantaneous pedestal values of $\beta^{ped}_e = 2\mu_0 p^{ped}_e / B^2_t$ versus ν^{ped}_{e*} of the four discharges in table 1 during the Q-EHO phase are shown (these correspond to the red points of figure 10).

As shown in figures 11(a) and (b), the pedestal density increase is accompanied by a temperature decrease where the pedestal knee appears to shift inwards, at least for the electron temperature. β^{ped}_e, where $\beta_e = 2\mu_0 p_e / B^2_t$ and $p_e = n_e T_e$, varies accordingly (cf figure 11(c)) with the Q-EHO phase sustained at $\beta^{ped}_e > 0.2\%$. This suggests that EHOs should be observed mainly in the high pressure region of the $n^{ped}_e - T^{ped}_e$ space. The evolution of the density and temperature profiles are associated with an increase of the pedestal collisionality leading to the loss of the EHO when $\nu^{ped}_{e*} \gtrsim 0.3$ (cf figure 11(c)), in line with the results in DIII-D and JT60-U [4, 15, 31]. Here ν_{e*} follows the definition of [32]

$$\nu_{e*} = 6.921 \times 10^{-18} \frac{q_{95} R_0 n_e Z_{eff} \ln \Lambda_e}{T^2_e \epsilon^{3/2}},$$

where ε is an effective inverse aspect ratio defined by $\epsilon = \frac{a}{R_0}\sqrt{\frac{1+\kappa^2}{2}}$ with R_0 and a the major and minor radii respectively with $a/R_0 \approx 0.33$, and $\ln \Lambda_e$ is the Coulomb logarithm. As pointed out in [5], plasmas with a higher percentage of impurities may require smaller pedestal densities in order to maintain the pedestal electron collisionality sufficiently small. Notice that the increase of pedestal collisionality is likely to yield a reduction of the bootstrap current, and a consequent increase of the local magnetic shear [32–35]. Hence, the collisionality threshold may be associated with a critical value of the magnetic shear below which EHOs can develop [36], in accordance with recent analytic and numerical modelling [18, 37–40].

Thus, EHO dynamics in JET appear to be governed primarily by β^{ped}_e and ν^{ped}_{e*}, both identifying a threshold for the EHO appearance, i.e. $\beta^{ped}_e > 0.2\%$ and $\nu^{ped}_{e*} < 0.3$ (see figure 11). Other parameters, such as q_{95} and the pedestal values of the magnetic shear, may play a role in the EHO triggering and their effect on the edge MHD behaviour this will be discussed in the following section.

3. JET-C and ILW ELMy database pedestal analysis

The aim of this section is to analyse the pedestal features of a database of JET discharges with carbon and ILW that, although partially fulfilling the parameter requirements for Q-EHO operation, are in ELMy regime. This would help in identifying if further hidden parameters, other than ν^{ped}_{e*} and β^{ped}_e discussed in the previous section, determine the accessibility to the ELMs/no-ELMs phase, and assessing if Q-EHO scenarios could potentially be reproduced in metallic machines.

The JET-C/ILW database under consideration consists of 1216 shots in high performance ELMing H-mode, divided into 360 shots with carbon wall and 856 shots with ILW [12]. Further details about this database can be found in [12]. The pedestal values of the associated physical quantities are averaged over a time window of 1–2 s during an inter-ELM stationary phase. Contrarily to the analysis of the previous section which focussed on the discharge evolution in the early phase when density is ramped (cf figure 1), the time window of all shots in the ELMy database is taken during the steady state flat-top. It is worth stressing that if EHOs exist in a transient phase, i.e. they are robust, they should be expected to be also observed

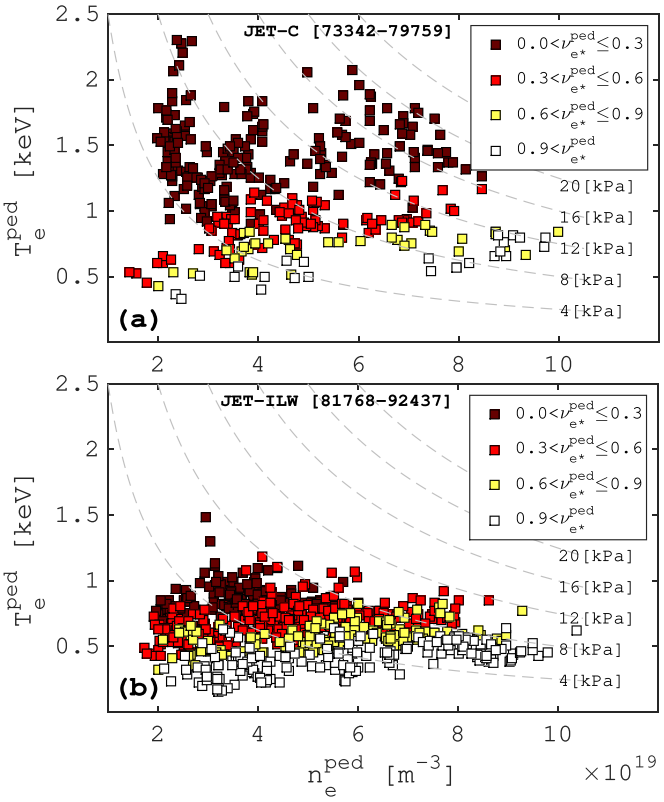

Figure 12. Scatter plot of JET carbon (a) and ILW (b) database discharges in the $n_e^{ped} - T_e^{ped}$ parameter space (each point corresponds to a pulse in the database). The dashed lines indicate the constant electron pressure levels, while bands of different pedestal electron collisionality are indicated by the colour associated with the discharge. Note that JET-C discharges exhibit larger pedestal T_e^{ped} and an associated smaller ν_{e*}^{ped} with a wider span in pedestal electron pressure. Note that the pulses of the ELMy database are a small subset of the JET carbon (from pulse #73342 to #79759) and ILW (from #81768 to #92437) experiments.

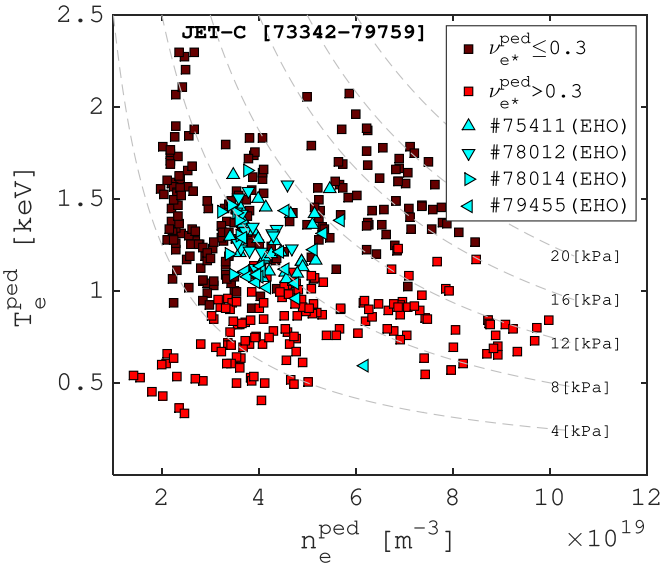

Figure 13. Plot of the JET-C points of figure 12(a) overlaid with the $n_e^{ped} - T_e^{ped}$ pedestal values (in cyan) of discharges of table 1 during the quiescent phase with EHOs. Note how the quiescent discharges tend to cluster in the region of high T_e and low n_e with electron pressure above ∼7 kPa, although there are no EHOs for pressure larger than 14 kPa regardless of n_e and T_e.

during a flat-top stage, if the plasma conditions required for their existence are met.

In analogy with figure 10, the pedestal electron temperatures plotted versus density for the shots in the database are shown in figure 12. At first glance, ILW discharges tend to occupy the lower part of the $n_e^{ped} - T_e^{ped}$ plane having on average lower temperatures, while exploring regions of similar densities. We observe that for these pulses the ion and electron temperatures have comparable values (i.e. $T_i \sim T_e$). We point out that within this database, high electron pressure regimes above 12 kPa are not explored by ILW discharges. As a direct consequence, from an inspection of the associated pedestal electron collisionality, we clearly see that ILW discharges tend to have higher ν_{e*}^{ped} values. Nevertheless, a reasonable number of ILW shots lie in a region of low to moderate collisionality at fairly high (low) electron temperature (density), where EHOs might be expected to exist.

As a first check, it is instructive to see whether the JET-C discharges in the database lie in the same region of the $n_e^{ped} - T_e^{ped}$ parameter space of the quiescent ones studied in the previous section. Hence, the $n_e^{ped} - T_e^{ped}$ data points of figure 12(a) are overlaid with the ones of figure 10 in section 2. This is shown in figure 13. It is immediate to notice that quiescent discharges occupy the region of the parameter space of high temperature and low density with the electron pressure above ∼7 kPa at low collisionality ($\nu_{e*}^{ped} \lesssim 0.3$ in line with DIII-D results [4]). It should also be noted that in figure 13 an upper limit in pressure ∼14 kPa appears where no EHOs are observed. As pointed out in section 2.5 (cf figure 11), beyond the small collisionality requirement, these results may suggest that quiescent EHOs phases are accessed when a threshold in the pedestal pressure is crossed. In addition, by comparing figures 12 and 13, the $n^{ped} - T_e^{ped}$ parameter space explored by JET-ILW shots seems not to overlap with the one of the JET-C Q-EHO discharges.

However, we notice that JET-C ELMy plasmas are found in regions where EHOs are expected to exist, i.e. despite having similar pedestal characteristics with the quiescent ones. Thus, we argue that other parameters must play a key role in determining whether or not the quiescent phase is accessible. We point out that when interpreting EHOs as pedestal localised pressure driven MHD instabilities [37, 39, 41], similarly to ballooning modes and to some extent Mercier modes, it is more appropriate to compare the pedestal β value rather than the pressure alone. This indeed is shown in figure 14, where the pedestal values of β_e, defined as in section 2.5, of the carbon and ILW database discharges are plotted against of ν_{e*}^{ped} (cf figure 11(c)). The green points in figure 14 and in the following figures highlight the database pulses, both carbon and ILW, which have $\nu_{e*}^{ped} < 0.3$ and $\beta_e^{ped} > 0.2\%$, whereas the red ellipse indicates the region in the $\nu_{e*}^{ped} - \beta_e^{ped}$ space which is explored by the discharges of table 1 of section 2.

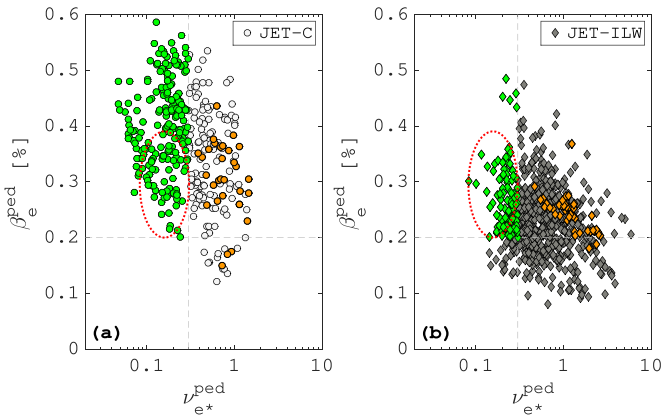

Figure 14. Scatter plot of the JET-C (a) and ILW (b) database of the pedestal values of β_e^{ped} vs ν_{e*}^{ped}. The grey horizontal dashed line indicates the $\beta_e^{ped} = 0.2\%$ level, while the vertical one denotes the $\nu_{e*}^{ped} = 0.3$ value. Carbon and ILW pulses of the database with $\nu_{e*}^{ped} < 0.3$ and $\beta_e^{ped} > 0.2\%$ are highlighted in green, whereas the orange points denotes shots having $3.2 < q_{95} < 3.5$ and $\delta > 0.37$. The red dashed ellipse indicates the region of the $\nu_{e*}^{ped} - \beta_e^{ped}$ space which is explored by the discharges of table 1 of section 2.

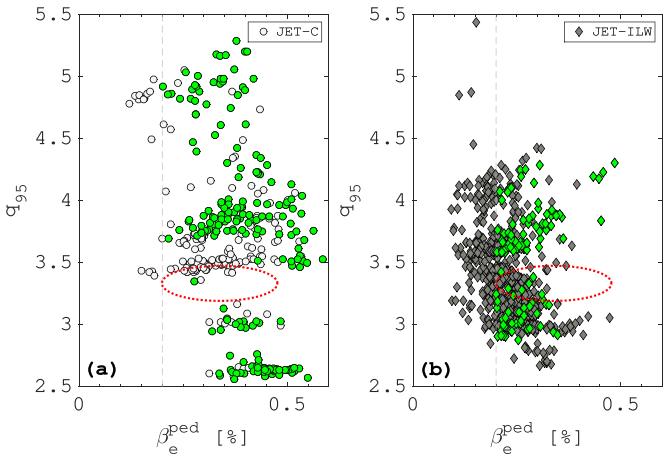

Figure 15. q_{95} vs pedestal β_e^{ped} scatter plot of the JET-C (a) and ILW (b) database pulses. The highlighted green points indicate shots with $\nu_{e*}^{ped} < 0.3$ and $\beta_e^{ped} > 0.2\%$ (cf figure 14). Discharges of table 1 occupy the region in the $\beta_e^{ped} - q_{95}$ space delimited by the red dashed ellipse. Note that only few points of the ELMy database with low ν_{e*}^{ped} and high β_e^{ped} span this region.

It is immediate to notice that JET-C discharges have a favourite access to high β_e^{ped} and low collisionality ($\nu_{e*}^{ped} \lesssim 0.3$) regions, whereas ILW shots tend to cluster mainly at high collisionality with lower β_e^{ped} (cf figure 12). In the space identified by the parameters given above, namely collisionality and β, the set of four discharges given in section 2 occupies the high-p_e^{ped} low-ν_{e*}^{ped} region which is well covered by the JET-C ELMy database, contrarily to the ILW shots which barely border it. Hence, as mentioned previously, other parameters must play a role in the determination of the quiescent/ELMy state.

Let us first point out that apart from the pedestal height (i.e. n_e^{ped}, T_e^{ped} and p_e^{ped}) and collisionality requirements, experiments in DIII-D, ASDEX-U and JT60-U showed that EHOs are obtained in plasmas with a sufficiently large edge-wall clearance. In DIII-D, ASDEX-U and JET, the plasma-wall gap is enhanced by having large values of triangularity, both upper and lower, whereas JT60 plasmas were able to operate with quiescent phases at low δ as long as a sufficient plasma-wall clearance was provided [6]. The necessity of the plasma-wall detachment is found to be a key ingredient for the EHO excitation in analytic modelling [37, 39] which also predicts the dependence upon the value of q in the pedestal in accordance with numerical simulations of JET-like plasmas [41, 42]. This dependence manifests itself by favouring the appearance of EHOs when q has a weakened shear and is close to a low m/n rational, as shown by the *exfernal model* of [37–39]. We might therefore expect EHOs when q_{95}, or more precisely q in the pedestal, takes particular values.

Thus, we identify four parameters that are likely to determine the accessibility to the quiescent regime with EHOs:

$$\beta_e^{ped},\ \nu_{e*}^{ped},\ \delta \text{ and } q_{95}. \qquad (1)$$

Note that apart from triangularity, all these quantities are local in nature, i.e. they specifically identify the pedestal conditions. It is worth to point out that although the plasma-wall clearance could be affected by elongation, the value of κ associated with the discharges in the JET-C/ILW database does not significantly differ from the one of the pulses reported table 1. As such, elongation can be regarded as a fixed parameter.

We expect that EHOs can be excited if the quantities associated with the database of figure 12 take simultaneously the same values of, or are close enough to, the ones of the quiescent discharges of table 1. Hence, for each discharge of the ELMy database we plot the parameters listed above against each other, analysing how they distribute with respect to the ones of the quiescent pulses of section 2. Since the $\beta_e^{ped} - \nu_{e*}^{ped}$ space has already been analysed in figure 14, we plot in figures 15–17 the remaining combinations of the parameters given in (1).

Let us point out that the ELMy pulses in the database are only a small subset of all the JET discharges within the range indicated in figure 12. Hence, the appearance of clusters in figures 15–17 is not due to the lack of experimental points, but rather to the database selection process.

Analysing where Q-EHO shots from table 1 locate in the parameter space identified by combining pair by pair the physical variables given in (1), shows (cf figures 14–17) that there is some overlapping with carbon ELMy pulses, whereas such overlap is less pronounced for the ILW ones. Such overlapping is further reduced when considering database discharges with $\nu_{e*}^{ped} < 0.3$ and $\beta_e^{ped} > 0.2\%$, and this is even more evident for ELMy ILW shots as shown in figures 15(b)–17.

In particular, we notice from figures 16 and 17 that ELMy database discharges with EHO compatible β_e^{ped}, ν_{e*}^{ped} and δ but different values of q_{95} (cf table 1) do not exhibit quiescent phases. Thus, we argue that the dependence upon q has to be a key ingredient in the mode excitation [31] (cf section 2). The role of q_{95}, however, is not clear since experiments in DIII-D have been observed not to have preferred values for q_{95},

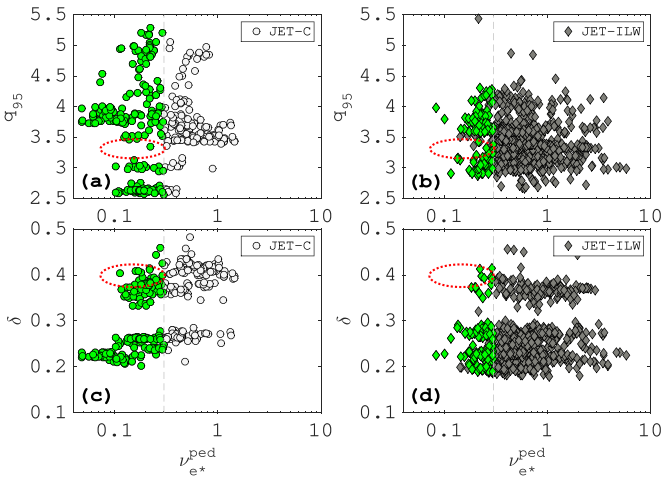

Figure 16. Scatter plot of q_{95} and δ vs pedestal ν^{ped}_{e*} for JET-C ((a) and (c)) and ILW ((b) and (d)) pulses of the ELMy database. The grey vertical line denotes the $\nu^{ped}_{e*} = 0.3$ value. The q_{95}, δ and ν^{ped}_{e*} parameters associated with JET-C pulses of table 1 fall in the region delimited by the red dashed ellipses. As in figure 15, only few points of the ELMy database with low ν^{ped}_{e*} and high β^{ped}_e fall inside these regions.

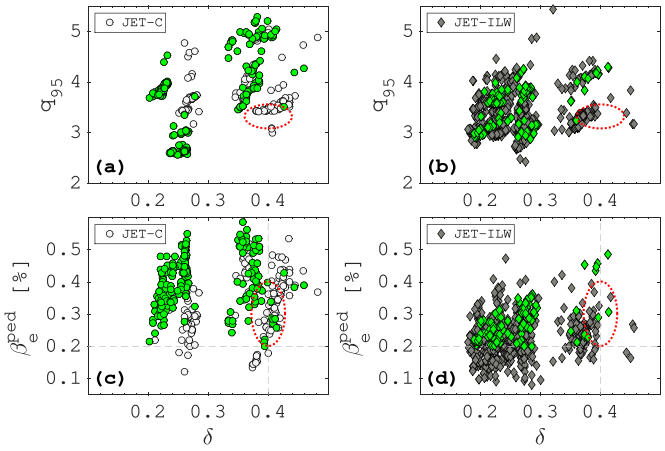

Figure 17. q_{95} and pedestal β^{ped}_e vs δ scatter plot of the JET-C ((a) and (c)) and ILW ((b) and (d)) database pulses. The red ellipse has the same meaning as in figure 16. Also in this case the ELMy database with EHO compatible ν^{ped}_{e*} and β^{ped}_e barely spans the regions explored by the pulses of table 1.

whereas ASDEX-U and JT60-U achieved quiescent phases only in a narrow range of q_{95} [31] similarly to the JET findings shown in this work. Nevertheless, as previously discussed, if EHOs are to be considered as a pedestal MHD phenomenon, q-pedestal rather than q_{95} is the relevant parameter which should be used for determining the Q-EHO phase access, among with the local value of the magnetic shear [40]. Note that q-pedestal and q_{95} have been shown to differ appreciably [43]. However, extracting information on the pedestal values of q and its shear proves to be rather difficult, and further analyses are required to characterise better the experimental role of the two parameters.

Hence, from the results presented above and inspecting particularly figure 14, we are induced to infer that EHOs have not been observed in the ELMy database of figure 12 because none of the pedestal parameters had simultaneously the values that are specific of the JET-C quiescent shots of table 1.

Finally, although EHOs have not been observed in the aforementioned database of ILW discharges, there are some indications from more recent experiments that EHOs might be seen with a metal wall. Indeed, brief edge magnetic oscillations have been observed in high performance pulses with strong NBI heating. The associated macroscopic parameters, e.g. shaping and pedestal values, are similar to the ones of the quiescent JET-C discharges of table 1. Further analyses are however required to have a unique mode identification. Additional support to the possibility of EHO activity in metallic machines comes from novel ASDEX-U findings, where EHOs have been observed, although transiently, in co-NBI heated pulses with the NBI applied before entering the high confinement phase [44]. Moreover, more recent experimental observations in ASDEX-U reported the presence of EHOs lasting for several hundreds of milliseconds, suggesting the possibility that such oscillations could be steadily sustained [13].

4. Conclusions

In this work we presented a detailed analysis of quiescent JET discharges exhibiting EHO-type MHD activity. These edge oscillations have been observed in the early phase of the discharge, during the density ramp when strong NBI heating is applied to a low density plasma. In line with previous results on other devices such as DIII-D and ASDEX-U, EHOs are observed at low collisionality [31] with the pedestal characterised by high temperatures and low density. The pedestal densities achieved in JET are three or four times larger compared to the ones required to sustain EHOs in DIII-D, ASDEX-U and JT60-U, despite the fact that similar values of collisionality, β_e and Z_{eff} are reported across these machines. The density ramp is accompanied by a decrease of the pedestal temperature, with the knee of T^{ped}_e exhibiting an inwards shift leading to an increase of the pedestal collisionality. Plasma toroidal rotation does not seem to have a significant role in determining the EHO stability (cf figure 8), and this also holds true for external magnetic perturbations generated by EFCCs with currents up to 1 kA. This leads us to infer that the EHO dynamics should be primarily determined by internal mechanisms driven by the pedestal values of temperature, density and current, the latter being strongly affected by bootstrap contributions whose fraction is in turn dictated by plasma temperature and density.

The quiescent phase with EHOs, which is sustained until $\nu^{ped}_{e*} \sim 0.3$ and with $\beta^{ped}_e > 0.2\%$, is lost when pedestal top plasma density reaches a threshold value of $\sim 4-5 \times 10^{19}$ (m^{-3}). No EHOs are observed below a pedestal electron pressure of $\sim$7 kPa. The pedestal β value recorded in JET is in line with the one achieved by DIII-D [4], i.e. $\sim$1% by allowing for T_i being approximately 30% larger than T_e.

The pedestal features associated with JET-C Q-EHO discharges have been consequently compared with the ones of a database of ELMy pulses with both carbon and ILW conditioning. Database pulses with ILW tend to operate at lower temperature and pressure compared to the carbon ones, and this is reflected by having a larger fraction of ILW shots at high collisionality. As a direct consequence, Q-EHO pulses overlap regions in the $n_e^{ped} - T_e^{ped}$ space that, within the ELMy database, are explored primarily by carbon and not ILW pulses. Beyond β_e^{ped} and ν_{e*}^{ped}, other important parameters which can influence the accessibility to the quiescent phase are the plasma-wall detachment, determined primarily by the triangularity, and the plasma current, i.e. q_{95}.

It is found that database discharges with quiescent compatible ν_{e*}^{ped} and β_e^{ped}, fail to have triangularity and q_{95} values falling in the range of those observed in JET-C with EHO pulses. On the other hand, ELMy pulses with δ and q_{95} values close to the ones of quiescent scenarios do not have the required pedestal collisionality and pressure to sustain the EHO. Although the role of q_{95} is not clear, as other devices achieved quiescent operation with EHOs without a preferred value of q_{95}, we are led to infer that the pulses of the ELMy database did not exhibit EHO activity because ν_{e*}^{ped}, β_e^{ped}, δ and q_{95} did not have simultaneously the specific values characterising QH discharges observed in JET-C. Nonetheless, by inspecting the ELMy database, we see that ILW discharges have the potential to explore parameter regions which are compatible with quiescent plasma operation, and indications of transient edge oscillations have been observed in more recent JET-ILW pulses. This is also supported by findings in ASDEX-U [13] which seem to point clearly to the possibility that QH regimes with EHOs could be accessible in metallic machines.

Further analyses are nevertheless required to better understand the impact of the pedestal q and other parameters, such as wall conditioning and input power, on the MHD dynamics in these scenarios, aiming at the steady sustainability of quiescent regimes in metallic devices.

Data availability statement

The data that support the findings of this study are available upon reasonable request from the authors.

Acknowledgments

This work has been carried out within the framework of the EUROfusion Consortium and has received funding from the Euratom research and training programme 2014–2018 and 2019–2020 under Grant Agreement No. 633053 and from the RCUK (Grant No. EP/T012250/1). To obtain further information on the data and models underlying this paper please contact PublicationsManager@ukaea.uk. The views and opinions expressed herein do not necessarily reflect those of the European Commission. This work was supported in part by the Swiss National Science Foundation.

ORCID iDs

D Brunetti https://orcid.org/0000-0001-8650-3271
C J Ham https://orcid.org/0000-0001-9190-8310
J P Graves https://orcid.org/0000-0002-7959-7959
E Lazzaro https://orcid.org/0000-0002-3291-8890
A Mariani https://orcid.org/0000-0003-0476-3825
C Wahlberg https://orcid.org/0000-0003-4680-9190
W A Cooper https://orcid.org/0000-0003-1989-1926
E R Solano https://orcid.org/0000-0002-4815-3407
L Frassinetti https://orcid.org/0000-0002-9546-4494
M Fontana https://orcid.org/0000-0002-7979-7483
A Kleiner https://orcid.org/0000-0002-5800-8027
G Bustos Ramirez https://orcid.org/0000-0002-8817-5344
E Viezzer https://orcid.org/0000-0001-6419-6848

References

[1] Leonard A W 2014 *Phys. Plasmas* **21** 090501
[2] Viezzer E 2018 *Nucl. Fusion* **58** 115002
[3] Burrell K H *et al* 2001 *Phys. Plasmas* **8** 2153
[4] Burrell K H *et al* 2005 *Phys. Plasmas* **12** 056121
[5] Suttrop W *et al* 2003 *Plasma Phys. Control. Fusion* **45** 1399
[6] Oyama N *et al* 2005 *Nucl. Fusion* **45** 871
[7] Solano E *et al* 2010 *Phys. Rev. Lett.* **104** 185003
[8] Nave M F F *et al* 1997 *Nucl. Fusion* **37** 809
[9] Nave G T A *et al* 1998 *Nucl. Fusion* **38** 179
[10] Perez C P *et al* 2004 *Nucl. Fusion* **44** 609
[11] Beurskens M N A *et al* 2013 *Nucl. Fusion* **53** 013001
[12] Frassinetti L *et al* 2021 *Nucl. Fusion* **61** 016001
[13] Viezzer E *et al* 2021 *47th EPS Conf. on Plasma Physics (Virtual Conf.)* (European Physical Society) p P1.1054
[14] JET Team (presented by Lomas P J) 1995 Operation for high performance in the new JET configuration *Plasma Physics and Controlled Nuclear Fusion Research 1994 (Proc. 15th Int. Conf. Seville, 1994)* vol 1 (Vienna: IAEA) p 211
[15] Chen X *et al* 2016 *Nucl. Fusion* **56** 076011
[16] Groebner R J *et al* 2001 *Nucl. Fusion* **41** 1789
[17] Sharapov S E *et al* 2006 *Nucl. Fusion* **46** S868
[18] Kleiner A *et al* 2019 *Plasma Phys. Control. Fusion* **61** 084005
[19] Burrell K H *et al* 2004 *Plasma Phys. Control. Fusion* **46** A165
[20] Suttrop W *et al* 2004 *Plasma Phys. Control. Fusion* **46** A151
[21] Garofalo A M *et al* 2011 *Nucl. Fusion* **51** 083018
[22] Haskey S R *et al* 2018 *Plasma Phys. Control. Fusion* **60** 105001
[23] Haskey S R *et al* 2017 *J. Instrum.* **12** C10013
[24] Kim J *et al* 1994 *Phys. Rev. Lett.* **72** 2199
[25] Liu F *et al* 2015 *Nucl. Fusion* **55** 113002
[26] Hughes J W *et al* 2018 *Nucl. Fusion* **58** 112003
[27] Wagner F 2007 *Plasma Phys. Control. Fusion* **49** B1
[28] Sauter O and Medvedev S Y 2013 *Comput. Phys. Commun.* **184** 293
[29] Burrell K H *et al* 2002 *Plasma Phys. Control. Fusion* **44** A253
[30] Chen X *et al* 2017 *Nucl. Fusion* **57** 086008
[31] Oyama N *et al* 2006 *Plasma Phys. Control. Fusion* **48** A171
[32] Sauter O *et al* 1999 *Phys. Plasmas* **6** 2834
[33] Saarelma S *et al* 2013 *Nucl. Fusion* **53** 123012
[34] Saarelma S *et al* 2012 *Nucl. Fusion* **52** 103020

[35] Kim S K *et al* 2020 *Nucl. Fusion* **60** 076022
[36] Brunetti D *et al* 2019 *46th EPS Conf. on Plasma Physics* (Milan: European Physical Society) p P1.1031
[37] Brunetti D *et al* 2018 *Nucl. Fusion* **58** 014002
[38] Brunetti D *et al* 2018 *J. Plasma Phys.* **84** 745840201
[39] Brunetti D *et al* 2019 *Phys. Rev. Lett.* **122** 155003
[40] Bustos Ramirez G *et al* 2021 *Plasma Phys. Control. Fusion* **63** 124004
[41] Zheng L J *et al* 2013 *Nucl. Fusion* **53** 063009
[42] Zheng L J *et al* 2013 *Phys. Plasmas* **20** 012501
[43] Garofalo A M *et al* 2015 *Phys. Plasmas* **22** 056116
[44] Meyer H *et al* 2019 *Nucl. Fusion* **59** 112014